Synthesis and Characterisation of Shape-Controlled Platinum Nanoparticles

A Thesis Submitted towards Partial Fulfilment of

BS-MS Dual Degree Program by

Dinesh Bulani

20121095

Under the guidance of

Prof. Manoj Neergat

Department of Energy Science and Engineering

Indian Institute of Technology Bombay

To

Department of Chemistry

Indian Institute of Science Education and Research Pune

Certificate

This is to certify that this dissertation entitled “Synthesis and characterisation of shape controlled platinum nanoparticles” towards the partial fulfilment of the BS-MS dual degree programme at the Indian Institute of Science Education and Research, Pune represents the research carried out by **Dinesh Bulani** (20121095) at IIT-Bombay under the supervision of **Prof. Manoj Neergat,** Dept. of Energy Science and Engineering during the academic year 2016-2017.

Dinesh Bulani

Prof. Manoj Neergat
(Thesis Supervisor)

Date: 30th March 2017

Declaration

I hereby declare that the matter embodied in the report entitled “Synthesis and characterisation of shape controlled platinum nanoparticles” are the results of the investigations carried out by me at the Department of Energy Science and Engineering, IIT Bombay, under the supervision of **Prof. Manoj Neergat** and the same has not been submitted elsewhere for any other degree.

Dinesh Bulani

Prof. Manoj Neergat
(Thesis Supervisor)

Date**:** 30th March 2017

Acknowledgement

I would like to express my heartfelt gratitude and special appreciation to my supervisor **Prof. Manoj Neergat** for providing me opportunity to work on my Master's thesis and my deep gratitude and special thanks to Mr. Ruttala Devivaraprasad, Mr. Arup Chakraborty**,** Mr. Tathagata Kar and all my labmates for their kind support and guidance during the project.

And lastly I want to thank my family members without their sacrifice and constant support this might not be possible.

Dinesh Bulani

Table of Contents

Table of Figures

List of Tables

List of Abbreviations

ORR	Oxygen reduction reaction
PAFC	Phosphoric acid fuel cell
BE	Bulk electrolysis
CSCV	Cyclic staircase voltammetry
PEM	Polymer electrolyte membrane
AFC	Alkaline fuel cell
RRDE	Rotating ring disk electrode
RHE	Reversible hydrogen electrode
PEFC	Polymer electrolyte fuel cell
SOFC	Solid oxide fuel cell
PVP	poly (N-Vinyl 2- Pyrrolidone)
CV	Cyclic voltammetry
MCFC	Molten carbonate fuel cell
XRD	X- Ray diffraction
TEM	Transmission electron microscopy

Abstract

Tetra hexahedral platinum nanoparticles are electrochemically synthesized using square wave potential technique on a polished glassy carbon electrode. At the same time, platinum nanosphere and multipod are synthesized using the chemical method. The as-prepared nanoparticles are characterized by High-resolution Transmission electron microscopy (HR-TEM). Thereafter, the catalyst is subjected to potential cycling in 0.5 M H_2SO_4 and is tested for its possible activity towards oxygen reduction reaction (ORR). The particle size is found to be in the order of THH > Multipod > nanosphere and the ORR specific activity is in the order of multipod > nanosphere > THH. Since the size of the THH Pt nanoparticles are very large, the surface to volume ratio is very less which leads to less number of active sites. On the other hand, multipods contain less number anion (HSO_4^-) adsorption sites than nanosphere and therefore have more number of oxygen adsorption sites and high specific activity towards ORR.

1. Introduction

Platinum has an important role in many applications. It acts as a catalyst in the reduction of gases which is a pollutant and emitted from automobiles, nitric acid synthesis, cracking of oil, and oxygen reduction reaction (ORR) in fuel cells. In all of these applications, Pt is used in the form of fine particles. It has established that the reactivity and selectivity of platinum nanoparticles are shape-dependent.

In electrocatalysis, since many reactions are structure sensitive, the understanding role played on catalytic reactivity by the surface structure is necessary. The nanoparticles in the catalyst are of size 1-20 nm. In case of nanoparticles, surface area to volume ratio and surface energy are maximised and helps to reduce its cost for use in large scale application. Researchers are working on nanocrystals of noble metals and their controlled synthesis, characterization, and potential applications.

Shape-controlled metal nanoparticles play a vital role in chemical reactions since it allows to tune electronic, optical, magnetic, and catalytic properties of a functional material. It is observed that most of the catalytic reactions are structure-sensitive, where selectivity and reactivity is strongly controlled by surface structure of nanoparticles.
In this work, tetrahexahedral (THH) Pt nanoparticles (NPs) are synthesized electrochemically using a step potential and square-wave potential procedure. Pt nanostructures in the form of spheres and multipods were also synthesized using chemical method, by coupling the polyol (ethylene glycol) reduction of a platinum precursor (H_2PtCl_6) with the Fe(II)/Fe(III) redox pair, PVP as a stabilizer and the adsorption of oxygen and nitrogen gases.

Shape-controlled nanoparticles synthesis was previously reported for magnetic/optical applications by Peng et al. [3]. Ascorbic acid, polyvinylpyrrolidone (PVP), citric acid, cetyltrimethylammonium bromide (CTAB), etc were used as capping agents, surfactants, complex stabilizing agents and reducing agents for the synthesis of the particles [2-4]. Particle growth is controlled in a particular desired orientation when the capping agents are specifically adsorbed on facets on initial nuclei [3]. Crystals of

different shapes are synthesized when they grow in a specific direction from the nuclei depending on the type of capping agent used [3].

The amount of Pt that is used at the cathode side, where the ORR takes place in fuel cell, is too high in relation to the available Pt resources. Therefore, the activity of the ORR catalyst based on the amount of Pt (or other platinum group metals (PGM)) becomes the bottleneck for the commercialization of fuel cell. Fuel cell differs from a typical battery although having similar characteristics and components. Available maximum energy for energy storage device i.e. battery is calculated by the amount of chemical reactants consumed. Fuel cell is able to generate electrical energy unless until the fuel and oxidants are supplied to the electrodes. In the case of fuel cell, oxidant (O_2 from air) is supplied to cathode whereas gaseous fuel is supplied to the anode which leads to the generation of the electric current due to occurring electrochemical reactions. The operating principle is shown in Figure 1.

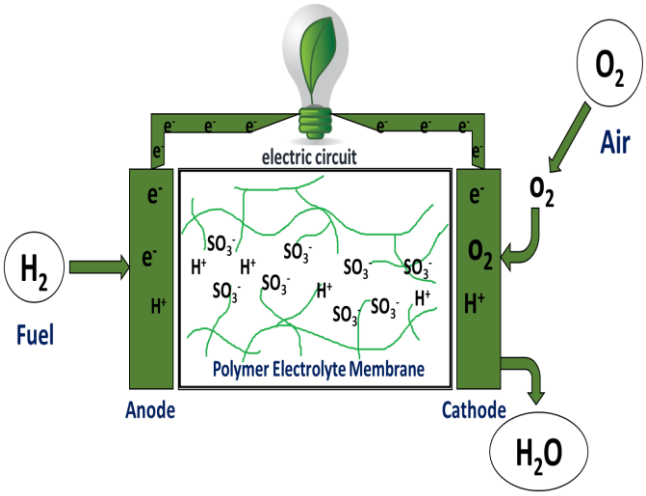

Figure 1 Operating principle of the fuel cell (taken from R. Devi with his permission)

..

Reactions occurring in a fuel cell:

$$\text{At anode: } 2H_2 \longrightarrow 4H^+ + 4e^- \quad (1)$$

$$\text{At cathode: } O_2 + 4H^+ + 4e^- \longrightarrow 2H_2O \quad (2)$$

$$\text{Cell reaction: } 2H_2 + O_2 \longrightarrow 2H_2O \quad (3)$$

It is observed that the rate of oxidation process (1) and reduction process (2) can be increased with the use of catalyst.

1.1 Brief history of fuel cell

It was known as early as 1839 that hydrogen and oxygen combine explosively to produce water and the reverse reaction, *i.e*., electrolysis of water was commercially used to produce oxygen and hydrogen. In 1800, Nicholson and Carlosle electrolyzed water for the first time. The formal discovery of the first fuel cell principle and making electricity from chemical is attributed to a British judge, Sir William Grove. He disconnected the electric source of a working electrolyser cell and passed hydrogen to one electrode and oxygen from air to the other electrode. On connecting the two electrodes together, a current was observed through the wire at a potential of 0.6 V, as long as hydrogen was given to the electrode. By connecting 50 cells together in series and supplying hydrogen to each, he managed to get around 25–30 V. Since then, significant research has been done and fuel cell technology has improved significantly. It is considered as the future option for zero emission technology in this global warming era.

1.2 Different types of Fuel cells

Classification of Fuel cells based on electrolytes

1. Polymer electrolyte fuel cells (PEFCs)
2. Alkaline fuel cells (AFCs)
3. Phosphoric acid fuel cells (PAFCs)
4. Molten carbonate fuel cells (MCFCs), and
5. Solid oxide fuel cells (SOFCs).

Operating temperature range of the fuel cell is governed by the electrolyte. Thermo mechanical and Physiochemical properties of materials used in fuel cell is governed by the operating temperature and useful life of a fuel cell.

Because of fast degradation and high vapour pressure at high temperature, the operation of fuel cells with aqueous electrolytes is limited to temperatures of about 200°C. The operating temperature plays an important role in the degree of fuel processing. All the fuel should be converted to hydrogen before entering the fuel cell and in low-temperature fuel cells anode catalyst is strongly poisoned by CO. Table 1 briefly explains the few main types of fuel cell characteristics.

Table 1 Characteristics of the main fuel cell types (The table is adopted from www.osti.gov)

	PEFC	**AFC**	**PAFC**	**MCFC**	**SOFC**
Electrolyte	Hydrated polymeric ion exchange membrane	Mobilized or immobilized potassium hydroxide in asbestos matrix	Immobilized liquid phosphoric acid in SiC	Immobilized liquid molten carbonate in $LiAlO_2$	Perovskites (ceramics)
Electrodes	Carbon	Transition metals	Carbon	Nickel and Nickel oxide	Perovskite and Perovskite / metal cermets
Catalyst	Platinum	Platinum	Platinum	Electrode material	Electrode material
Interconnect	Carbon or metal	Metal	Graphite	Stainless steel or Nickel	Nickel, ceramic, or steel
Operating temperature	40–80˚C	65–220˚C	205˚C	605˚C	600–1000˚C
Charge carrier	H^+	OH^-	H^+	CO_3^{-2}	O^{-2}
External reformer for hydrocarbon fuels	Yes	Yes	Yes	No, for some fuels	No, for some fuels
Prime cell components	Carbon-based	Carbon-based	Graphite-based	Steel-based	Ceramic
Product water management	Evaporative	Evaporative	Evaporative	Gaseous product	Gaseous product
Product heat management	Process gas + liquid cooling medium	Process gas + electrolyte circulation	Process gas + liquid cooling medium or steam generation	Internal reforming + process gas	Internal reforming + process gas

Here, it can be noticed that the fuel cells operating at low temperature require platinum as catalyst. Low durability and high cost are the most challenging issues in the commercialization of fuel cell and platinum-based catalysts are the major contributor to cost of fuel cell [5-7]. By using nano-sized catalyst, the cost can be reduced since it

offers high surface area. As the kinetics of the reduction process involves higher complexity, it is necessary to understand the detailed mechanism of the oxygen reduction process before designing the material for higher activity and cost efficiency.

We have prepared shape controlled Pt nanoparticles and analysed the samples using TEM, because it offers information about the atomic arrangement of the nanoparticles. The electrochemical properties of the as-prepared shape-controlled Pt nanoparticles were studied using cyclic voltammetry (CV) and rotation disk electrode (RDE). CV is usually used to characterise the electrochemically active surface. Catalytic current measured from RDE can eliminate the unexpected effect of oxygen diffusion, which is more intrinsic to represent the catalytic activity. These two techniques are usually combined together and have been demonstrated to be an appropriate model for fuel cell systems [8].

2. Literature review

The critical element in developing economically viable fuel cell is the discovery of proficient and commercially inexpensive catalysts for use in electrochemical energy conversion reactions such as hydrogen oxidation reaction and ORR.

2.1 Oxygen reduction reaction (ORR)

It is the most significant reaction involved in energy conversion in fuel cells. It proceeds by two pathways in the aqueous solutions: First one being the direct reduction of O_2 to H_2O by the transfer of four electrons. While, in the second pathway, O_2 is converted to H_2O_2 through the transfer of two electrons, followed by conversion of H_2O_2 to H_2O. It has been reported that the conversion of O_2 to superoxide (O_2^-) is also possible in the case of non-aqueous aprotic solvents. It is a reasonably complex reaction and includes several intermediates. These complications depend upon several factors such as the catalyst and also the electrolyte. The standard thermodynamic electrode potential is governed by the nature of electrolyte. These potential values are shown in Table 2.

Table 2 The electrode potentials for the reduction of O_2 [8,9].

Electrolyte	ORR reactions	Thermodynamic electrode potential at standard conditions, V
Acidic aqueous solution	$O_2 + 4H^+ + 4e^- \longrightarrow$ HOH	1.229
	$O_2 + 2H^+ + 2e^- \longrightarrow H_2O_2$	0.70
	$H_2O_2 + 2H^+ + 2e^- \longrightarrow$ 2HOH	1.76
Basic aqueous solution	$O_2 + HOH + 4e^- \longrightarrow 4OH^-$	0.401
	$O_2 + HOH + 2e^- \longrightarrow HO_2^- + OH^-$	-0.065
	$H_2O^- + H_2O^+ + 2e^- \longrightarrow 3OH^-$	0.867

Non-aqueous aprotic solvent	$O_2 + e^-$ ⟶ O_2^- $O_2^- + e^-$ ⟶ O_2^{-2}	a b

Here, ‘a’ represents the reduction potential to create superoxide (O_2^-) and ‘b’ shows the reduction potential for the conversion of superoxide to peroxide. These values vary from one solvent to another.

Depending on the applications, these three different types of reduction processes which involve one, two and four electron-transfer have specific importance. The transfer of four electrons is preferable in the fuel cells. The production of H_2O_2 is governed by the reduction pathway which involves the transfer of two electrons. In a similar way, the reduction pathway which comprises one electron-transfer has the highest importance in the investigation of the ORR mechanism.

2.2 ORR mechanism on Platinum

The catalytic ORR is a complex mechanism which involves several elementary steps and intermediates. H_2O_2 and H_2O are the products of the simplified mechanism of the particular reduction. The ORR on Pt catalysts includes several individual reactions, as shown in **Fig. 2**. Rotating ring disk electrode (RRDE) measurements study ensures that reduction pathway which involves four electron-transfer is the major process occurring on the Pt surface. It is also observed that the reduction process is the same for both acidic and alkaline aqueous electrolytes [10].

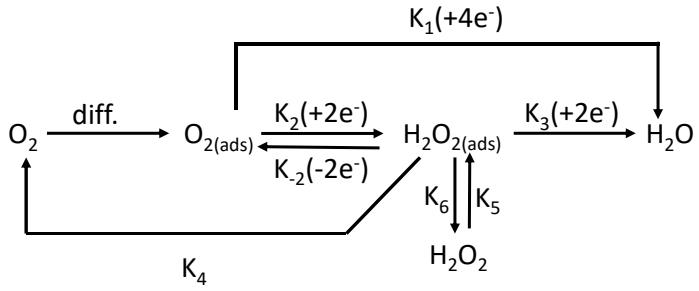

Figure 2 Scheme of oxygen reduction on platinum surface (adapted from Rampino et al.) [12].

Here k_1 represents the rate constant for the direct conversion of O_2 to water by the transfer of four electrons. Another mechanism involves a two steps reduction in which k_2 represents the rate constant for the formation of $H_2O_{2\,(ads)}$ from $O_{2(ads)}$ through a two electron transfer mechanism. K_3 denotes the rate constant for formation of water from $H_2O_{2(ads)}$. K_4 signifies the rate constant for the chemical decomposition of the $H_2O_{2(ads)}$ on the electrode. K_5 represents the desorption rate constant of $H_2O_{2\,(ads)}$. Steps involved in the mechanism are shown below:

$$O_2 + * \longrightarrow O_2^* \quad (4)$$

$$O_2^* + H^+ + e^- \longrightarrow HO_2^* \quad (5)$$

$$HO_2^* + H^+ + e^- \longrightarrow H_2O + O^* \quad (6)$$

$$O^* + H^+ + e^- \longrightarrow OH^* \quad (7)$$

$$OH^* + H^+ + e^- \longrightarrow H_2O + * \quad (8)$$

The detailed study of the ORR mechanism suggests that the adsorption of oxygen and expulsion of hydroxide ion from the platinum surface are the rate determining steps. The exposed facets governs the performance of the Pt nanoparticles in the reduction processes [11, 12].

3. Experimental methods

3.1 Chemicals

The precursors (H_2PtCl_6, and K_2PtCl_4), PVP and Ethylene glycol used in the synthesis were procured from Alfa Aesar. The solvents used for washing the samples (acetone, ethanol and hexane) were purchased from Merck.

3.2 Electrochemical preparation of THH platinum nanoparticles

The electrochemical preparation of THH Pt NPs was carried in a conventional three electrode cell. Before the electrodeposition of the THH Pt NPs, the GCE was mechanically polished using alumina polish of 0.05 and 0.1 micron in size. Subsequently, the electrode was cleaned in an ultrasonic bath with Millipore water. The THH NPs were electrodeposited onto the GC disk in a 0.4 mM K_2PtCl_4 + 0.1 M H_2SO_4 electrolyte solution using Wave Driver Bipotentiostat (WaveDriver 20, Bipotentiostat from Pine Instruments with AfterMath software which was installed on a Windows 10 system) [13]. The GCE was immersed into the argon-saturated electrolyte and was held at 1.15 V for 60 seconds. Then the electrode was rotated at 100 rpm to ensure mass transport of the ions and a potential step was applied from 1.15 to -0.15 V for 0.1 s to deposit Pt nuclei. The conversion of the nuclei into THH Pt NPs was done by square-wave potential (f = 100 Hz) for different duration with a lower potential limit (E_L) of 0.0 V and an upper potential (E_U) of 1.15 V, respectively.

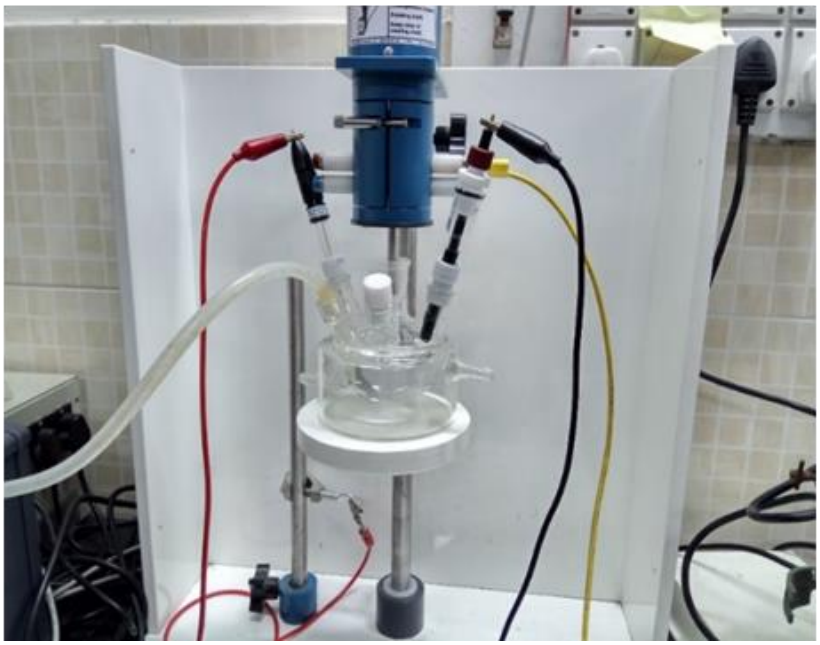

Figure 3 Setup of synthesis and electrochemical characterization of platinum THH NPs.

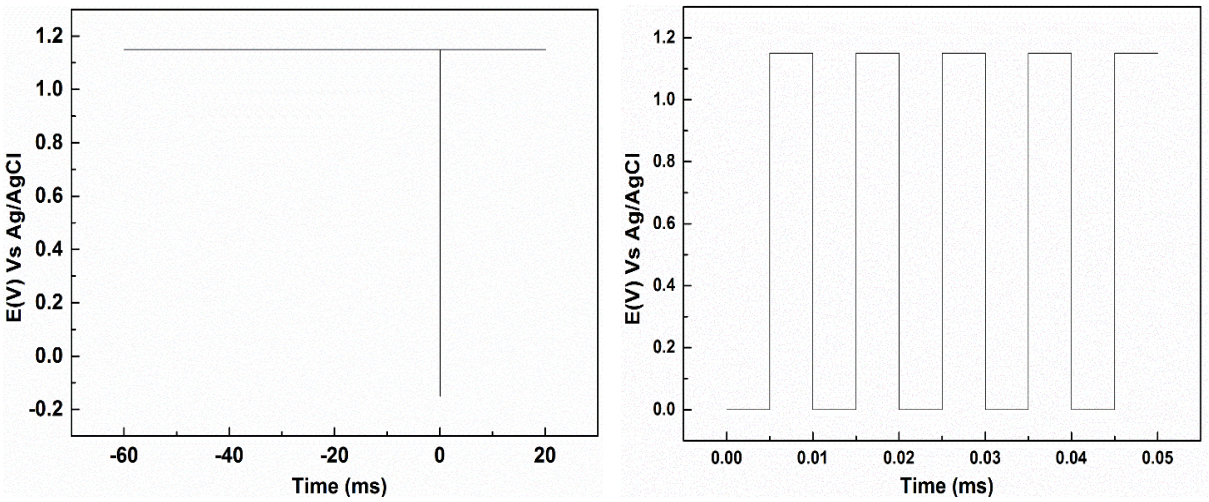

Figure 4 Step potential through bulk electrolysis technique at rotation rate of 100 rpm. Initially held at 1.15 V for 60 second (induction period) then step at -0.15 V for 0.1 second (electrolysis period) and again at 1.15 V for 20 second (relaxation period). **(b)** Square wave potential done through cyclic staircase voltammetry. Initial potential (E_L) = 0 V, upper potential (E_U) = 1.15 V, f = 100 Hz, Amplitude = 1.15 V, square width = 5 ms.

3.3 Experimental method for nanosphere and multipod

In this synthesis, ethylene glycol (4 ml) was taken in a three-neck flask, containing a magnetic stirring bar, attached with a reflux condenser. The contents was heated in presence of air at 110°C in silicon oil bath for 1 h in a fume hood to remove any trace water; reaction vessel was closed using a rubber septum. 33 mg H_2PtCl_6 and 45 mg poly vinyl pyrrolidone were taken separately and added to ethylene glycol (2 ml) at room temperature and sonicated till the salt dissolved. The two EG solutions were then added drop-wise with the help of pipette, simultaneously to the reaction flask. The reaction mixture was heated at 110 °C in air till solution changed from golden orange to green–yellow. It shows the formation of Pt(II) species as the intermediate. For nanosphere synthesis nitrogen was purged for 0.5 h through the reaction mixture and changed its colour to brown and finally dark brown [14].

For the synthesis of branch-shape of Pt nanoparticles, same procedure was followed as above. $FeCl_2$. $4H_2O$ (50 mM) 20 μL was added after Pt(II) formation (approximate 1.5 hr) and reaction mixture was heated in presence of N_2 for 1 hr, finally, solution turned dark brown.

3.4 Cleaning step

In both cases, the product was collected by centrifuging several times at 15000 rpm for 10 minutes with ethanol, acetone, and n-hexane to clean ethylene glycol and excess PVP. The precipitate was collected and electrochemically characterised by voltammetry and physically characterised by TEM, and HRTEM.

3.5 Electrode preparation

Collected sample was taken in a cleaned vial with ethanol and it was kept in oven at 80°C. DI water was added to the dried sample and it was sonicated for 30 minutes to get a fine free flowing catalyst ink. 3 drop of 10 μL solution was casted on a glassy carbon electrode (as shown in image) and it was left for drying overnight**.**

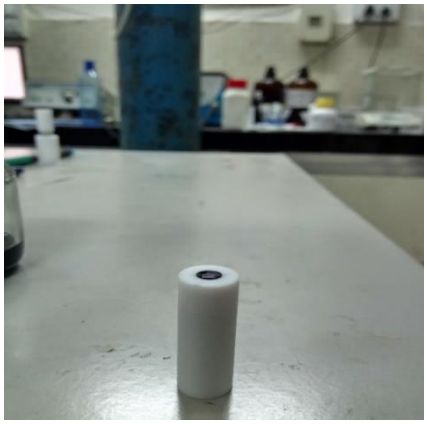

Figure 5 Glassy carbon electrode with drop casted platinum nano particles.

4. Results and discussion

4.1 Electrochemical and Physical Characterization of synthesized THH Platinum nanoparticles

As we know hydrogen adsorption/desorption is finger print to analyse the surface structure of Pt NPs. So to analyse surface structure, THH nanoparticle were deposited on a glassy carbon electrode and the cyclic voltammograms were recorded in an electrochemical cell. The potential was handled using a Wave Driver Bipotentiostat (WaveDriver 20, Bipotentiostat from Pine Instruments with AfterMath software which was installed on a Windows 10 system). A platinum wire was taken as the counter electrode and Ag/AgCl was taken as the reference electrode. Initially, 0.5 M H_2SO_4 solution was purged with argon for 30 minutes prior to recording cyclic voltammograms (CVs) at a scan rate of 50 mV sec^{-1}**.**

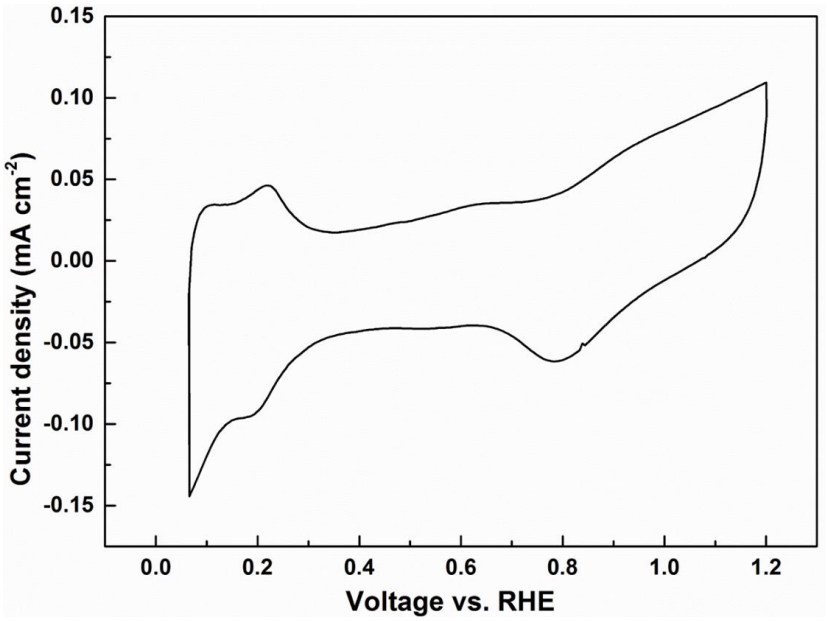

Figure 6 The CV of THH Platinum nanoparticle in 0.5 M H_2SO_4 solution recorded at a scan rate of 50 mV s^{-1}.

The CV shows good precious metal features with hydrogen adsorption and desorption ($H_{ads}/_{des}$) region upto 0.4 V, double layer region 0.4-0.7 V, and then oxide formation region above 0.7 V. In the CVs, two peaks are observed at 0.1 V and at 0.22 V. As the

surface of synthesized shape-controlled nanoparticles are made of facets with different $H_{ads/des}$ energy, peak features are observed at specific potentials and, the hydrogen under potential deposition (H_{upd}) features depend on shape of the nanoparticles. Because of adsorbtion of Hydrogen ions and HSO_4^- anions, voltammetric features of catalysts are different.

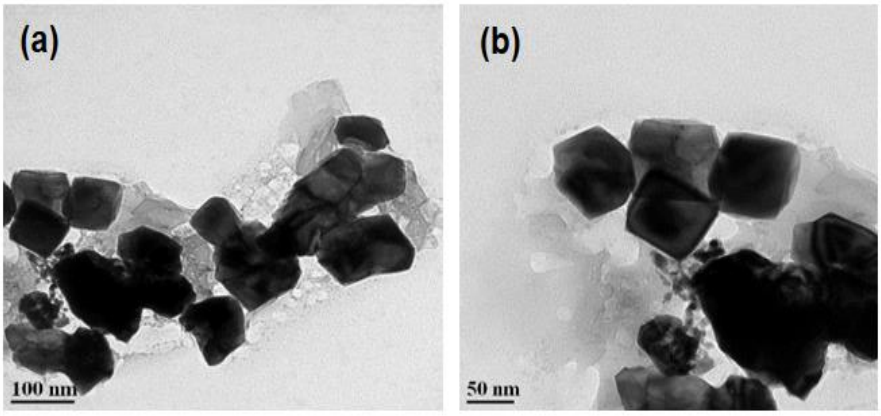

Figure 7 TEM images of THH Pt NPs in which Square wave potential is given for 15 mins.

From above TEM images and CVs, it can be concluded that the shape-control of nanoparticles limited. To improve nanoparticle shape selectivity, different methods were adopted. At different square wave potential time which is responsible for growth, we got improved features in cyclic voltammogram and TEM images.

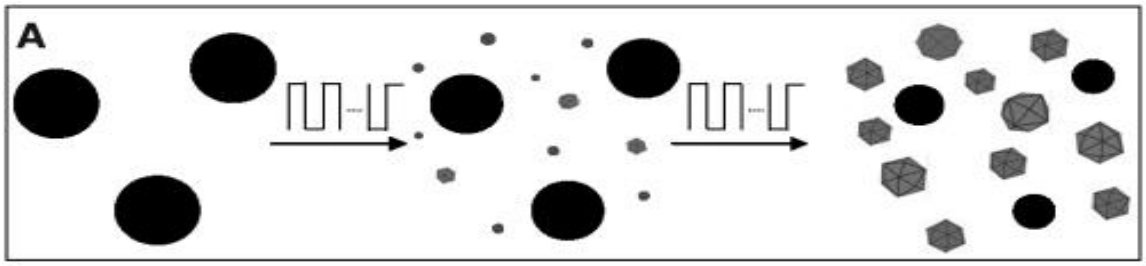

Figure 8 Selectivity improvement with square wave potential time. (adapted from Tian et al.)[13].

.

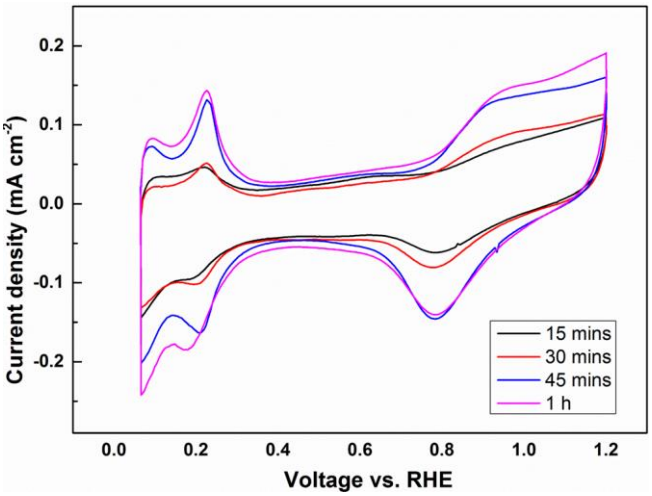

Figure 9 Cyclic voltammograms of the platinum nanoparticles taken at different time of square wave recorded at scan rate of 50 mV sec^{-1} in 0.5 M H_2SO_4.

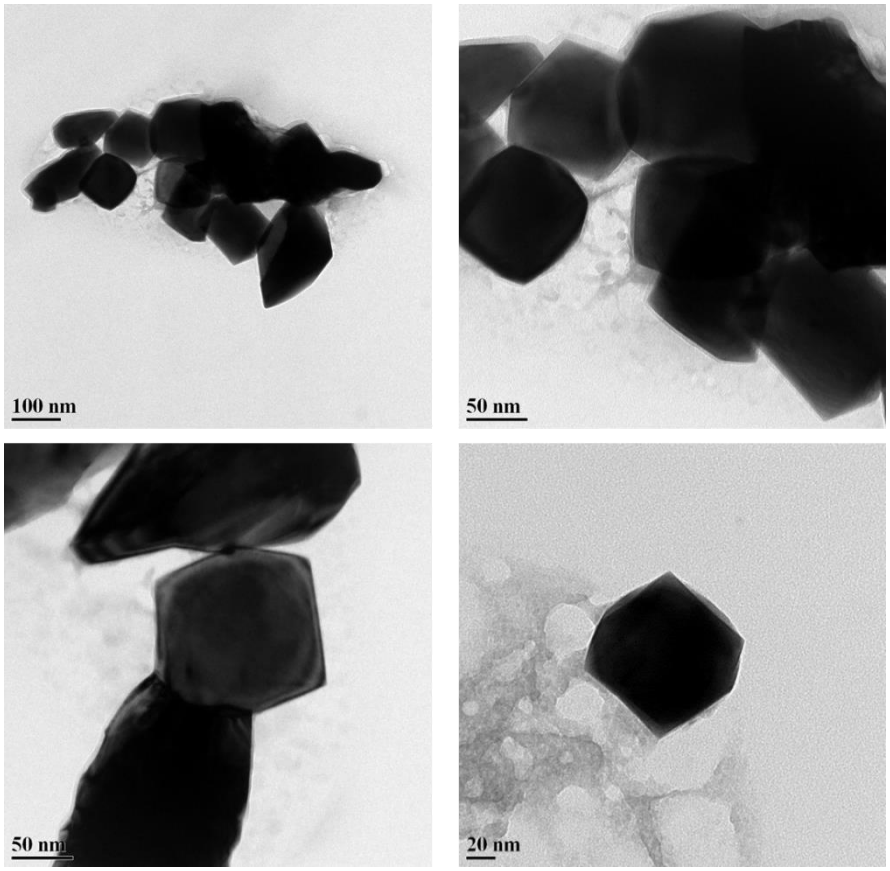

Figure 10 TEM images of sample in which square wave potential is given for 30 mins

From Figures 9 and 10, the shape selectivity of the nanoparticles is dependent on the square wave potential duration. As square wave potential time is increased, the peak intensity of both Hupd peaks in CVs (0.1 V and 0.22 V) (Figure 9) increases and in

Figure 10 THH particles are less agglomerated than figure 7 for most of the region of Cu grid and for same concentration.

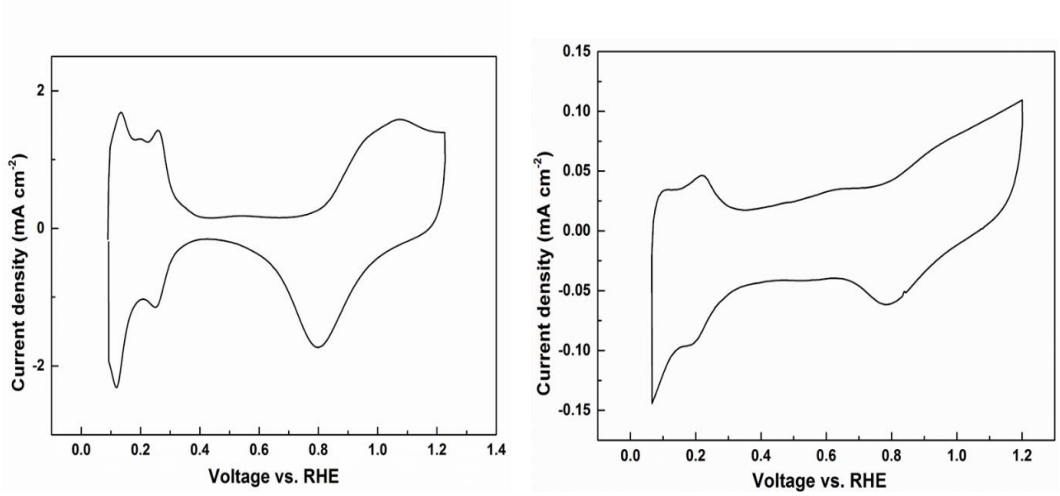

Figure 11 Comparison of the cyclic voltammograms (CVs) of polycrystalline Pt NPs [15] and THH Pt NPs recorded in argon-saturated 0.5 M H_2SO_4 electrolyte solution at scan rate 50 mV sec^{-1}.

To show that particles have shape like reported polycrystalline Pt, we compare the CVs of THH Pt NPs and PC Pt. The CVs are recorded in 0.5 M H_2SO_4 electrolyte. The CV of PC Pt displays the well-known properties of polycrystalline Pt or “standard” Pt NPs found in fuel cell catalysts [16, 17] which is similar of synthesized THH Pt nanoparticles (containing all three region as in Polycrystalline Pt). Potential region up to 0.4 V vs. RHE, called the Hupd (underpotentially deposited hydrogen) region, the current correlates to hydrogen adsorption (negative scan direction) and desorption (positive scan direction), respectively. The Hupd features at 0.1 V RHE are more pronounced than the ones at 0.3 V RHE. This is in opposite to the CV of the THH Pt NPs where first peak is less intense than second peak. The different features indicate difference in surface morphology of both samples.

4.2 Proposed formation process of THH nanoparticles

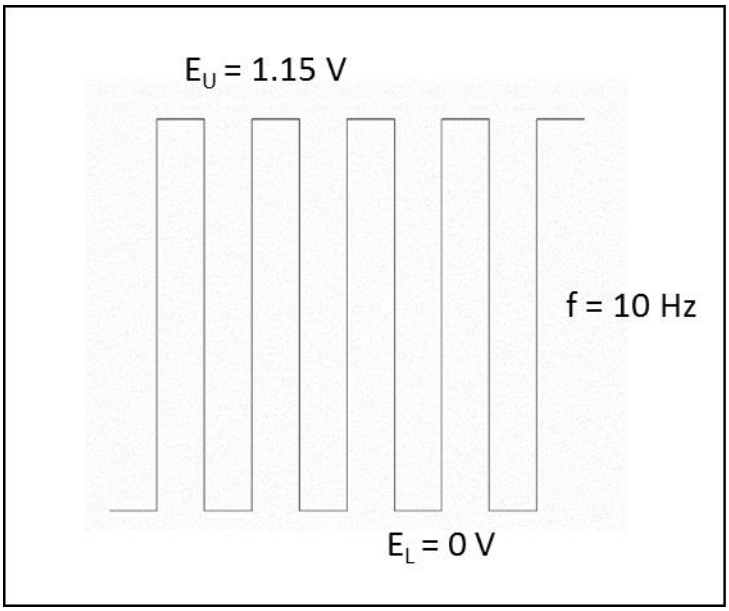

Figure 12 Square wave potential used for THH Pt nanoparticle synthesis.

At Upper voltage (E_u) 1.15 V, the following electrochemical oxidation reactions may occur on Pt surface as reported by Conway et al. [18,19]:

$Pt + H_2O \rightarrow PtOH_{ad} + H^+ + e^-$ (9)

$PtOH_{ad} \rightarrow PtO_{ad} + H^+ + e^-$ (10)

$PtO_{ad} + 2H^+ \rightarrow PtO_2 + 2H^+ + 2e^-$ (11)

$PtO_{ad} + H_2O \rightarrow PtO_2 + 2H^+ + 2e^-$ (12)

Here, $PtOH_{ad}$ and PtO_{ad} (O_{ad} means adsorbed oxygen) are the adsorbed oxygen species on Pt surface and Pt^{2+} is free ions that can diffuse to the GC surface
At lower potential (E_L) 0 V the corresponding reduction reactions may occur:

$PtOH_{ad} + H^+ + e^- \rightarrow Pt + H_2O$ (13)

$PtO_{ad} + 2H^+ + 2e^- \rightarrow Pt + H_2O$ (14)

$PtO_2 + 4H^+ + 2e^- \rightarrow Pt^{2+} + H_2O$ (15)

$Pt^{2+} + 2e^- \rightarrow Pt$ (16)

During square wave potential treatment, the reaction (9)-(16) occur periodically, as reported by Tian et al. The reaction (16) can result in the growth of new Pt NCs on GC surface through nucleation and growth due to the fast migratory ability of free Pt^{2+} ions. The reaction (9) and (10) correspond to the adsorption of oxygen on Pt, and reaction (13) and (14) correspond to the desorption of oxygen on Pt. These two periodically repeated processes determine that the exposed facets of the newly grown NCs are high-index facets, i.e. the particle shape is THH [13].

4.3 Characterization of chemically prepared platinum nanoparticles

Cyclic voltammograms of chemically synthesized platinum nanoparticles were recorded in 0.5 M H_2SO_4. Figure 14 shows CVs of platinum multipod particles. As shown, H_{upd} area, double layer and oxide regions increase with cycling.

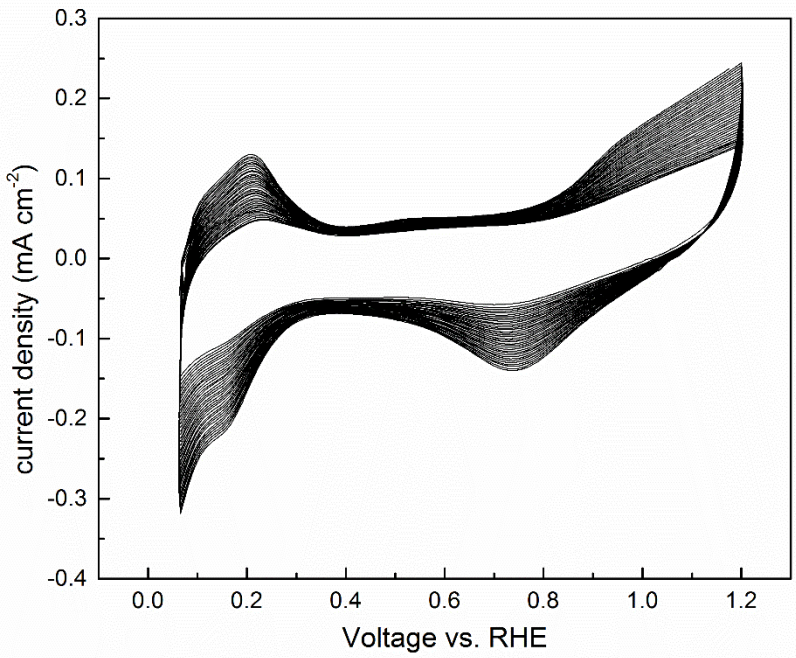

Figure 13 voltammogram of platinum multipod recorded in 0.5 M H_2SO_4.

4.3.1 Comparison of cyclic voltammograms of nanosphere and multipod Pt nanoparticles in 0.5 M H_2SO_4

Figure 14 Shows the cyclic voltammograms of the nanosphere and multipod Pt nanoparticles in 0.5 M H_2SO_4 at 50 mVs^{-1} scan rate. It is possible to identify the main voltammetric features in this electrolyte. The broad peaks at 0.11 V and 0.20 V with Pt nanosphere and multipod particles originate from the (200) and (111) exposed facets. The current at 0.22 V in the CV of nanosphere Pt is more than that in the CV of multipod Pt.

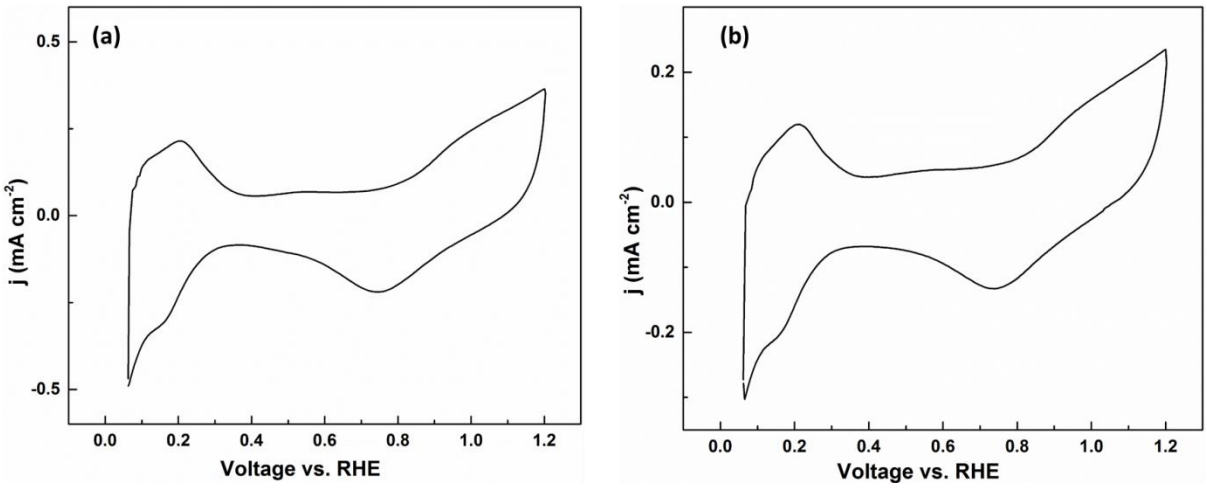

Figure 14 Cyclic voltammograms of (a) nanosphere and (b) multipod Pt nanoparticles in 0.5 M H_2SO_4.

4.3.2 TEM analysis of chemically synthesized Pt nanoparticles

Figure 15 shows TEM images of Pt nanospheres when the Pt(II) intermediate was reduced under nitrogen atmosphere and no Fe(II) species was present. The spherical nanoparticles have average diameter of 4-5 nm (as shown in figure 17 (a)). Figure 16 shows the TEM image of the synthesized platinum nanoparticles in which 50 mM Fe(II) were added after Pt(II) formation. Particle size is bigger in this case with an average size of 7-8 nm (as shown in figure 17 (b)) and the particles start to branch into multipod shape. From TEM images, the selectivity for nanosphere is more than 90% and for multipod ~ 40%.

As shown in (HRTEM image d) Figure 15 and 16, d spacings of both particles are 0.23 nm and 0.19 nm corresponding to (111) and (200) directions, respectively. Which also show crystal packing is in FCC because miler indices are all even or all odd.

After addition of H_2PtCl_4 and PVP, the solution is heated for 1.5 h in air and its colour changes from yellow-orange to green yellow which shows Pt(II) formation. Within 1 h, spherical Pt NPs of size 4-5 nm are produced if this reaction allowed to continue in air atmosphere at 110 °C. In such a case, once some Pt nuclei form in the solution phase, Pt(II) reduction is accelerated by an autocatalytic process [21]. Reduction of Pt(II) to Pt(0) is faster under nitrogen atmosphere than in air and in 30 mins spherical NPs are formed. This observation suggests that in the absence of nitrogen, oxygen adsorbtion take place onto the surface of Pt nuclei and slow down the autocatalytic reaction, still, reaction was too fast in presence of oxygen.

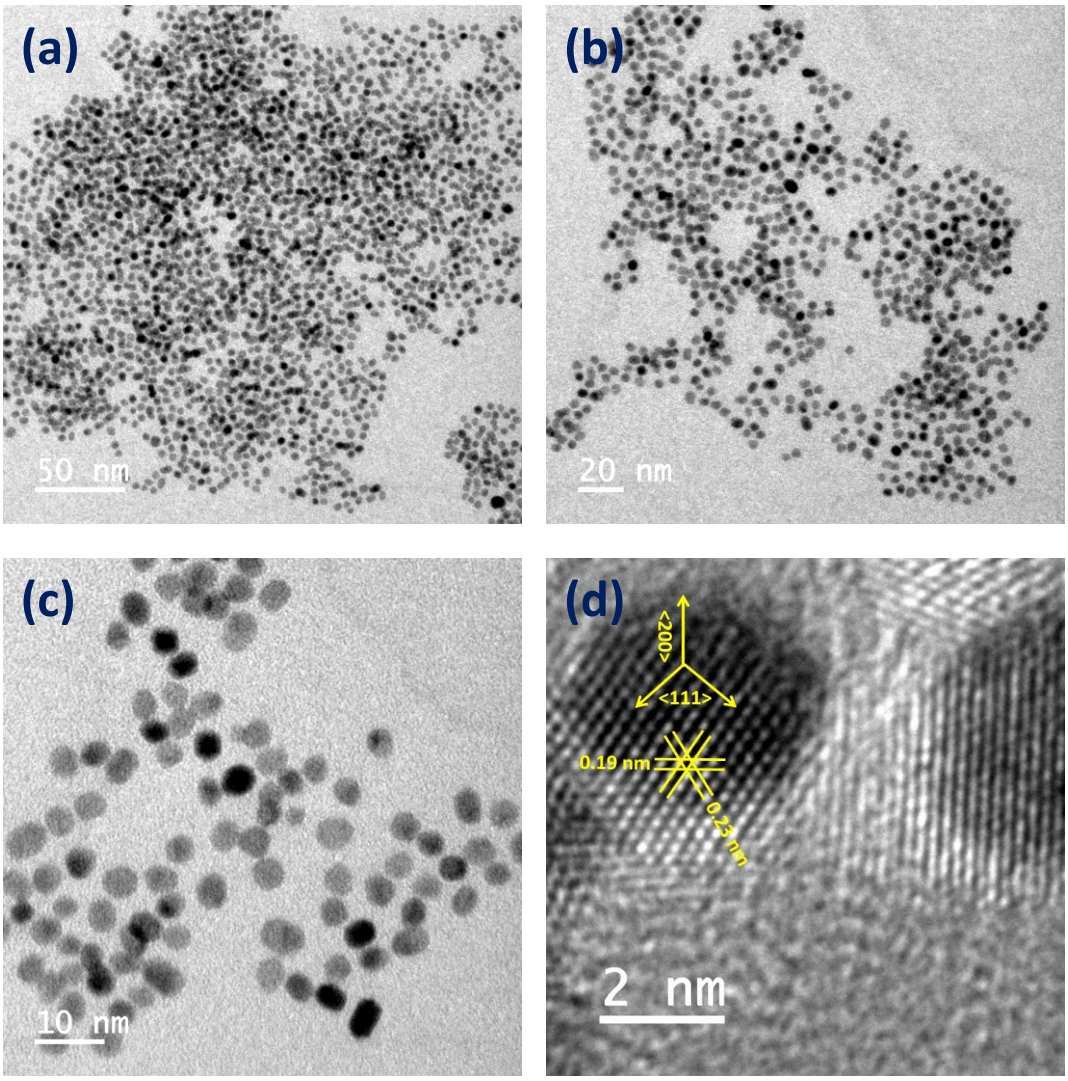

Figure 15 TEM images of platinum nanosphere synthesized using H_2PtCl_6, PVP and Ethylene glycol, (a) 50 nm (b) 20 nm (c) 10 nm (d) 2 nm.

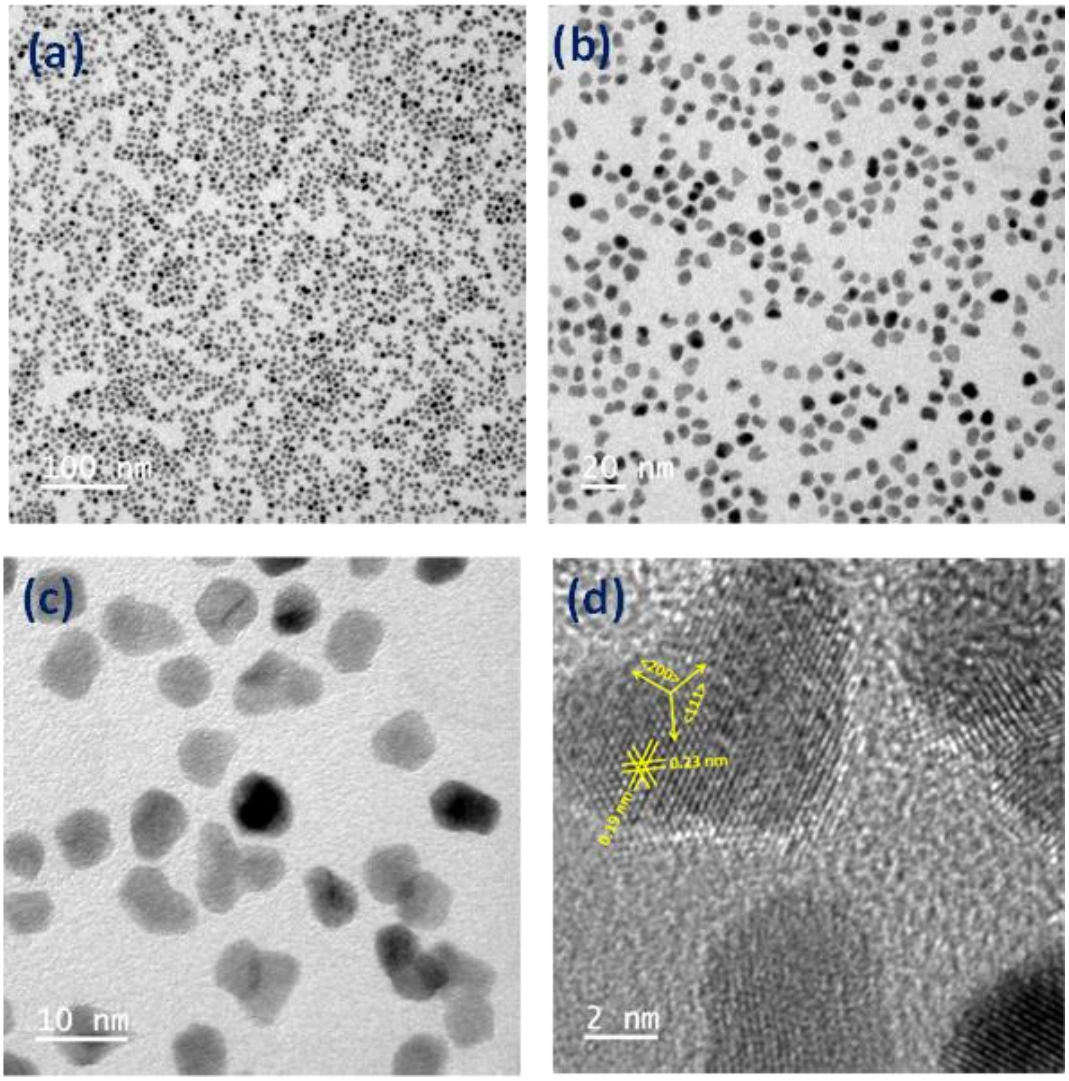

Figure 16 TEM images of Platinum multipod synthesized using H_2PtCl_6, PVP, Ethylene glycol and trace amount of $FeCl_2.4H_2O$ (a) 100 nm (b) 20 nm (c) 10 nm (d) 2 nm.

In presence of Fe(II) or Fe(III) in reaction mixture, reduction of Pt(II) gets slower. Because Fe(II) get oxidized in presence of oxygen to Fe(III) which further oxidize Pt nuclei back to Pt(II) and decreases the super-saturation of the Pt atoms. Fe(III) converts to Fe(II), and only very small amount of Fe is needed for the synthesis; therefore, both Fe(II) and Fe(III) ions can be used. This suggests that oxygen is responsible for slowing down the growth through etching mechanism and surface adsorption when coupled with the Fe(II)/Fe(III) species. It is difficult to identify which effect is dominant because both are strongly dependent on the Fe(II)/Fe(III) species

and concentration of oxygen. Rate of reduction of the Pt(II) species can be regulated using these two [22].

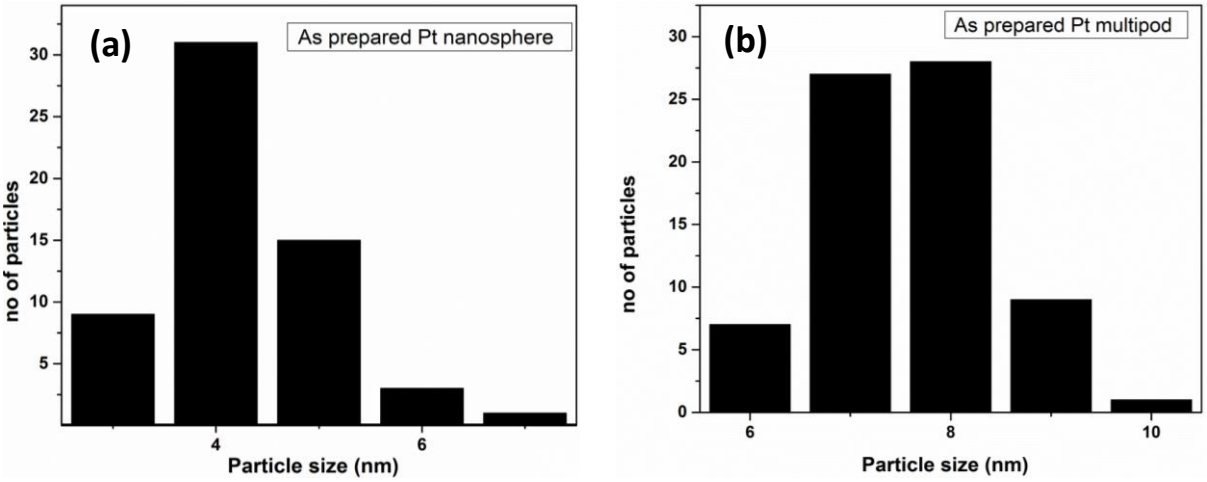

Figure 17 Histogram obtained from TEM images of platinum nanosphere and multipod.

4.4 Comparison of ORR activity of Pt THH, multipod and nanosphere in 0.5 M H_2SO_4

Figure-18 Shows the ORR voltammograms of THH, Multipod, Nanosphere shaped Pt nanoparticles in 0.5 M H_2SO_4. The most accurate comparison of ORR kinetics is in the potential region of 0.8 to 0.9 V. It is easily seen from the voltammograms that there is some variation in crystal faces, The ORR activity order of synthesized all three nanoparticles in sulfuric acid is due to the strong adsorbtion of the HSO_4^- anion. Specific activity of nanoparticle in 0.5 M H_2SO_4 of THH is least and for multipod is more than nanosphere. Because THH nanoparticle higher in size than multipod and nanosphere so we can say due to less surface to volume ratio oxygen adsorbtion decrease, multipod is more active than nanosphere because multipod have less anion adsorbtion so more sites for oxygen adsorption[23].

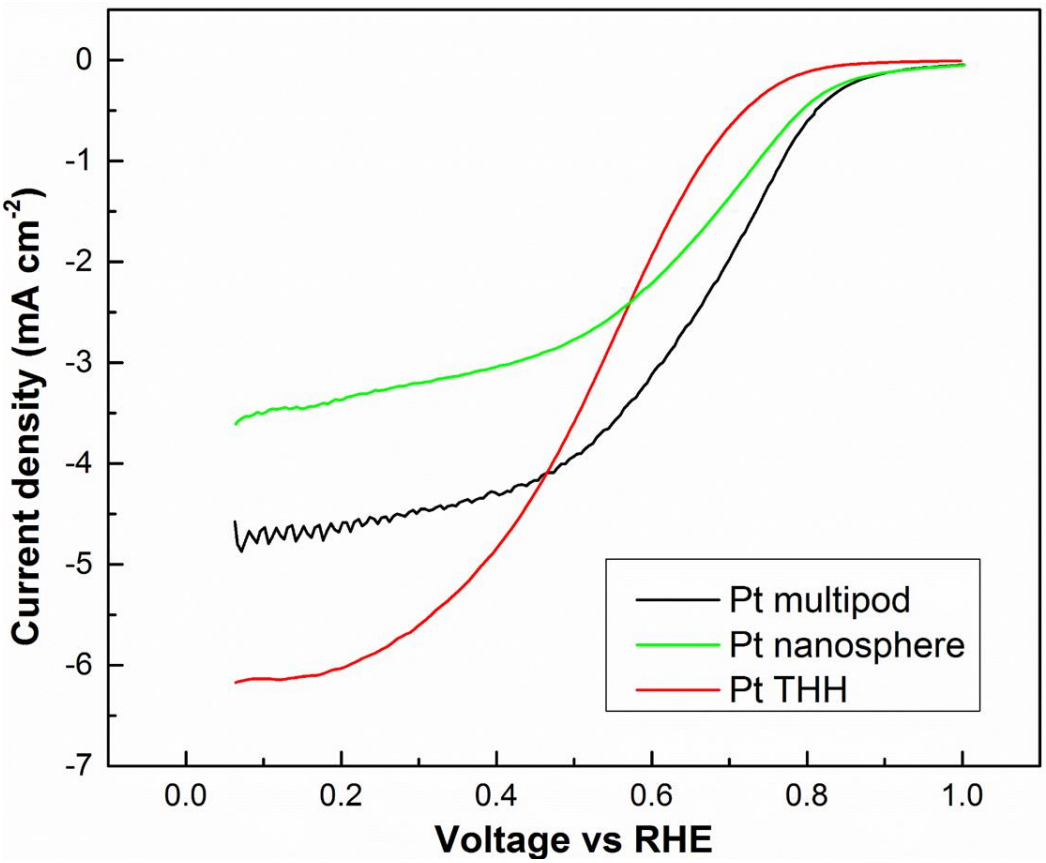

Figure 18 ORR voltammograms of nanosphere, multipod and THH shaped Pt nanoparticles in 0.5 M H_2SO_4 at 20 mV sec^{-1} scan rate and 1600 rpm rotation rate in O_2-saturated solution.

(100)-Site-dominated Pt nanoparticles show higher ORR activity when compared with that of (111) sites because HSO_4^- adsorb specifically on ordered (bi) dimensional sites at 0.5 V. At higher potential reduce the adsorbtion of oxygen or oxygenated species [24]. So we can also say multipod have (100) dominated site and nanosphere have (111) dominated sites.

5. Conclusions

THH platinum nanoparticles were synthesized using electrochemical method and sphere and multipod shaped Pt nanoparticle were synthesized using chemical method. The morphology of these nanoparticles is characterised with voltammetry and TEM. The voltammetric features obtained with different shape-controlled Pt nanoparticles correlates with the *ex-situ* TEM. The ORR activity order in 0.5 M H_2SO_4 was Pt multipod > Pt nanosphere > Pt THH. The electrocatalytic properties are strongly dependant on the size and shape of the nanoparticles, in a similar way to what was established from fundamental studies with Pt single crystal electrodes.

Proper cleaning procedure of chemically prepared nanoparticles, selectivity improvement of THH and multipod Pt nanoparticles and size reduction of THH Pt nanoparticles yet to be done.

6. References

1. Y. Xia, Y. Xiong, B. Lim, S.E. Skrabalak, Shape-Controlled Synthesis of Metal Nanocrystals: Simple Chemistry Meets Complex Physics, *Angew. Chem., Int. Ed*. 2009, 48, 60−103.

2. J. Chun-Jiang, F. Schuth, Colloidal Metal Nanoparticles as a Component of Designed Catalyst, *Phys. Chem. Chem. Phys*., 2011, 13, 2457−2487.

3. Z. Peng, H. Yang, Designer Platinum Nanoparticles: Control of Shape, Composition in Alloy, Nanostructure and Electrocatalytic Property, *Nano Today* 2009, 4, 143−164.

4. J. Chen, B. Lim, E. P. Lee, Y. Xia, Shape-Controlled Synthesis of Platinum Nanocrystals for Catalytic and Electrocatalytic Applications, *Nano Today,* 2009, 4, 81−95.

5. D. B. Meadowcroft, Low-Cost Oxygen Electrode Material, *Nature,* 1970, 226, 847–848.

6. H. A. Gasteiger and N. M. Markovic, Just a dream-or future reality?, *Science* 2009 324, 48–49.

7. G. M. Whitesides, and G. W. Crabtree, Don't Forget Long-Term Fundamental Research in Energy, *Science*, 2007, 315, 796–798.

8. E. Yeager, Dioxygen Electrocatalysis Mechanism in Relation to Catalyst Structure, *J. Mol. Catal.,* 1986, 38, 5–25.

9. A. J. Bard, and L. R. Faulkner, Electrochemical Methods and Fundamental Applications, New York, Wiley 1980

10. A. A. Balandin, Problems of Chemical Kinetics*,* Catalysis and Reactivity, Academy of Sciences, Moscow 1955.

11. N. M. Markovic and P. N. Ross, Surface Science Studies of Model Fuel Cell Electrocatalysts, *Surf. Sci. Rep.,* 2002, 45**,** 117–229.

12. Rampino, and F. F. Nord, Preparation of Platinum and Palladium Synthetic High Polymer Catalysts and the Relationship Between Particle Size and Rate of Hydrogenation, *J. Am. Chem. Soc.,* 1942, 63, 2745–2749.

13. N. Tian, Z. Y. Zhou, S. G. Sun, Y. Ding, Z. L. Wang, Synthesis of Tetrahexahedral Platinum Nanocrystals with High-Index Facets and High Electro-Oxidation Activity, *Science,* 2007, *316*, 732.

14. J. Chen, T. Herricks, and Y. Xia, Polyol Synthesis of Platinum Nanostructures: Control of Morphology through the Manipulation of Reduction Kinetics, *Angew. Chem. Int. Ed.,* 2005, 44, 2589 –2592

15. R. Devivaraprasad, T. Kar, A. Chakraborty, R.K. Singh, M. Neergat, Reconstruction and dissolution of shape-controlled Pt nanoparticles in acidic electrolytes, *Physical Chemistry Chemical Physics,* 2016, 18, 11220-11232.

16. K.J.J. Mayrhofer, B.B. Blizanac, M. Arenz, V.R. Stamenkovic, P.N. Ross, N.M. Markovic, The Impact of Geometric and Surface Electronic Properties of Pt-Catalysts on the Particle Size Effect in Electrocatalysis, *J Phys Chem B*, 2005, 109, 14433-14440.

17. K. Shinozaki, J.W. Zack, R.M. Richards, B.S. Pivovar, S.S. Kocha, Oxygen Reduction Reaction Measurements on Platinum Electrocatalysts Utilizing Rotating Disk Electrode Technique, *J. Electrochem. Soc.*, 2015, 162, 1144-1158.

18. D.A.J. Rand, R. Woods, A study of the Dissolution of Platinum, Palladium, Rhodium and Gold Electrodes in 1 M Sulphuric Acid by Cyclic Voltammetry, *J. Electroanal. Chem.,* 1972*,* 35, 209-218.

19. B. E. Conway, Electrochemical Oxide Film Formation at Noble Metals as a Surface-Chemical Process, *Prog. Surf. Sci.,* 1995*,* 49, 331-452.

20. N. Furuya, M. Shibata, Structural Changes at Various Pt Single Crystal Surfaces with Potential Cycles in Acidic and Alkaline Solutions, *J. Electroanal. Chem.,* 1999*,* 467, 85.

21. J. M. Petroski, Z. Wang, T. C. Green, M. A. El-Sayed, Kinetically Controlled Growth and Shape Formation Mechanism of Platinum Nanoparticles, *J. Phys. Chem*. B, 1998, 102, 3316-3320.

22. J. Chen, T. Herricks, and Y. Xia, Polyol Synthesis of Platinum Nanostructures: Control of Morphology through the Manipulation of Reduction Kinetics, *Angew. Chem. Int. Ed*. 2005, 44, 2589 –2592.

23. R. Devivaraprasad, R. Ramesh, N. Naresh, T. Kar, R.K. Singh and M. Neergat Oxygen Reduction Reaction and Peroxide Generation on Shape-Controlled and Polycrystalline Platinum Nanoparticles in Acidic and Alkaline Electrolytes, *Langmuir* 2014, 30, 8995−9006.

24. N. M. Markovic, H. A. Gasteiger, P. N. Ross, Oxygen Reduction on Platinum Low-Index Single-Crystal Surfaces in Sulfuric Acid Solution: Rotating Ring-Pt(hkl) Disk Studies, *J. Phys. Chem*., 1995, 99, 3411−3415.